available at www.sciencedirect.com

ScienceDirect

journal homepage: www.elsevier.com/locate/compag

Vision-based localization of a wheeled mobile robot for greenhouse applications: A daisy-chaining approach

S.S. Mehta[a,b,*], T.F. Burks[a], W.E. Dixon[b]

[a] The Department of Agricultural and Biological Engineering, University of Florida, Gainesville, FL 32611, United States
[b] The Department of Mechanical and Aerospace Engineering, University of Florida, Gainesville, FL 32611, United States

ARTICLE INFO

Article history:
Received 24 January 2007
Accepted 8 January 2008

Keywords:
Daisy chaining
Wheeled mobile robot (WMR)
Greenhouse
Vision-based localization

ABSTRACT

The Euclidean position and orientation of a wheeled mobile robot (WMR) is typically required for autonomous selection and control of agricultural operations in a greenhouse. A vision-based localization scheme is formulated as a desire to identify the position and orientation of a WMR navigating in a greenhouse by utilizing the image feedback of the above-the-aisle targets from an on-board camera. An innovative daisy chaining strategy is used to find the local coordinates of the above-the-aisle targets in order to localize a WMR. In contrast to typical camera configurations used for vision-based control problems, the localization scheme in this paper is developed using a moving on-board camera viewing reseeding targets. Multi-view photogrammetric methods are used to develop relationships between different camera frames and WMR coordinate systems. Experimental results demonstrate the feasibility of the developed geometric model.

1. Introduction

A greenhouse is defined as a house of glass, polycarbonate or fiberglass construction used for propagation, growth and care of plants. The function of a greenhouse is to create the optimal growing conditions for the full life of the plants (Badgery-Parker, 1999). The main application of robots in the commercial sector has been concerned with the substitution of manual human labour by robots or mechanized systems to make the work more time efficient, accurate, uniform and less costly while reducing/eliminating the occupational health hazard towards the human labor.

With recent advances in camera technology, computer vision, and controls theory, application of wheeled mobile robots (WMR) has shown growing interest towards automation of greenhouse agricultural operations such as pesticide/fungicide spraying, health monitoring, de-leafing, etc. In Sammons et al. (2005), an autonomous mobile robot for use in pest control and disease prevention application for a commercial greenhouse has been described where human health hazards are involved in spraying potentially toxic chemicals in a confined space. Van Henten et al. (2004) described the autonomous de-leafing process of cucumber plant using a mobile robot. A virtual prototype of a service robot for health monitoring and localized chemical, drugs and fertilizers dispensing to plants in greenhouses has been realized in Acaccia et al. (2003). Acaccia et al. (2003) described the functionality of a mobile robot as a service robot but the localization scheme for the robot has not been presented. Dario et al. (1994) described a vision-based navigation of a wheeled mobile robot for operations such as picking of ripe tomatoes and spraying of flowers.

Most of the past research focuses on a particular, spatially non-varying task to be performed by the autonomous system in a greenhouse. However, for a large greenhouse spa-

* *Corresponding author at*: The Department of Mechanical and Aerospace Engineering, University of Florida, Gainesville, FL 32611, United States. Tel.: +1 352 283 4741.
E-mail address: siddhart@ufl.edu (S.S. Mehta).
0168-1699/$ – see front matter © 2008 Elsevier B.V. All rights reserved.
doi:10.1016/j.compag.2008.01.013

tial control over the agricultural operations might be desired (e.g. selective spraying of pesticides along different aisles of a greenhouse) requiring the knowledge of the Euclidean position and orientation (i.e. pose) of a WMR. Different localization schemes are aimed at providing an autonomous system with the knowledge of the Euclidean environment as well as their real-time states and positions to navigate in the specified task space. Typically, the states of the robots are provided by the use optical encoders, gyroscopes, acceleration sensors, speedometers, etc., while the localization information is acquired by calculating the accumulative position data.

The dead reckoning system represents a low cost robot localization method that integrates wheel translation and rotation to determine the robot's Euclidean pose. However, due to initial position errors and disturbance during the motion, the cumulative effects of the small error can result in a large error in the robot's position estimate. A relocalization method based on evidence grids is presented in Yamaucbi (1996) to compensate for the errors introduced by wheel slippage. But expensive multiple sensors are required for establishing the evidence grid for the robot. A WMR localization system based on perpetual sensors such as ultrasonic sensors, GPS, infrared sensors, imaging systems, etc., can provide a vivid and more accurate view of the Euclidean environment. Many researchers fusing the dead reckoning and perpetual sensors measurements are provided in Aono et al. (1988); Tsai (1998); Ashokaraj et al. (2004). However, the constructed localization system is more complex, also the environmental measurement and data processing is computationally expensive. A large group of navigation systems use rangefinders for simultaneous localization and mapping (SLAM). In many solutions, Kleeman and Kuc (1995); ldzikowski et al. (1999); Skrzypczyfnski and Drapikowski (1999); Zhang and Ghosh (2000) it is assumed, that the Euclidean environment consists of the objects/obstacles and the shape of these objects can be defined by geometric primitives like line, arc, etc. A localization scheme based on 3D laser rangefinder (LRF) is presented in Idzikowski and Podsedkowski (2005), but enforces the restriction on the robot movement to a planar motion. In Ohno and Tadokoro (2005), Ohno et al. proposed a method of dense 3D map building and discrete robot motion estimation using SLAM based on 3D scan matching. The dense 3D map is generated using LRF data and color image fusion. Often the pose of a WMR is determined by a global positioning system (GPS) or inertial measurement unit (IMU). However, GPS may not be available in many environments and accuracy of GPS positioning may not be sufficient, and IMUs can drift and accumulate errors over time in a similar manner as dead reckoning.

Given recent advances in the image extraction/interpretation technology, an interesting approach to overcome the pose measurement problem is to utilize a vision system. A simple localization scheme based on the image feedback from a global-camera is presented in Guo et al. (2006), where a pose of a particular robot in a WMR formation can be determined based on the identifier of a robot. Multiple mobile robot navigation method using the indoor global positioning system is proposed by Hada and Takase (2001). In Hada and Takase (2001), WMR localization is achieved by using cameras distributed in the robot working domain.

In this paper, an innovative daisy chaining approach (Mehta et al., 2006) is utilized for the localization of a WMR in a greenhouse while utilizing the image feedback from a WMR on-board monocular camera. The moving on-board cameras attached to a WMR are used to provide pose measurements of the WMR relative to the greenhouse inertial frame of reference

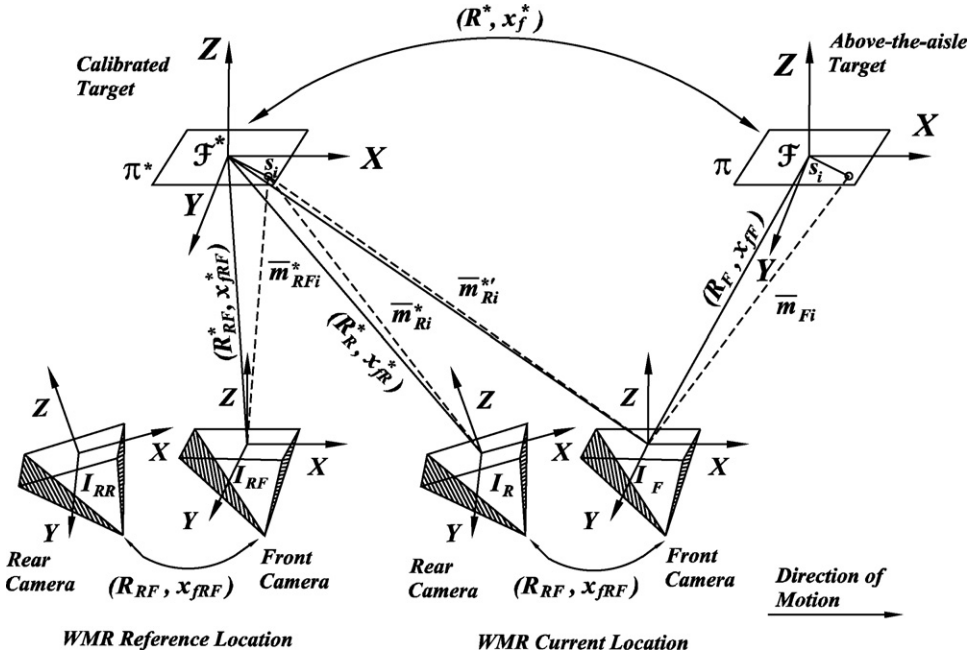

Fig. 1 – Camera coordinate frame relationships: the moving on-board monocular camera system (coordinate frame $\mathcal{I}_{RF}$ at reference location, coordinate frame $\mathcal{I}_F$, coordinate frame $\mathcal{I}_R$) navigating below the calibrated reference target (coordinate frame $\mathcal{F}^*$) identifies the pose of a WMR. The position and orientation of above-the-aisle target (coordinate frame $\mathcal{F}$) is determined using image feedback from $\mathcal{I}_F$ and $\mathcal{I}_R$.

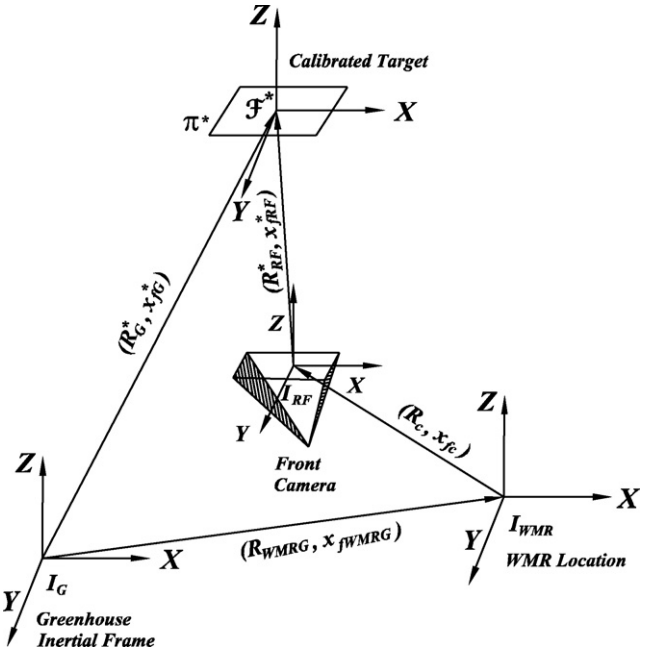

Fig. 2 – Localization of a WMR (coordinate frame $\mathcal{I}_{WMR}$) with respect to greenhouse inertial frame of reference (coordinate frame $\mathcal{I}_G$) while viewing the calibrated target (coordinate frame $\mathcal{F}^*$).

while utilizing image feedback of above-the-aisle targets. The contribution of this paper is the development of a localization scheme for a WMR using two monocular on-board cameras resulting in a larger field-of-view. Geometric constructs developed for traditional camera-in-hand problems are fused with fixed-camera geometry to develop a set of Euclidean homographies, which can be decomposed using standard decomposition algorithms to determine the pose of a WMR.

2. Geometric model

Consider a two monocular camera system, comprising of a forward and reverse looking camera, on-board a WMR that is navigating along a planar motion while capturing the image data of the overhead (i.e. above-the-aisle) target objects as depicted in Figs. 1 and 2. The moving coordinate frames $\mathcal{I}_F$ and $\mathcal{I}_R$ are attached to the forward and reverse looking on-board cameras, respectively, and the coordinate frame $\mathcal{F}$ is attached to above-the-aisle targets. The target is represented in the camera image by four[1] feature points that are coplanar and not colinear. The Euclidean distance (i.e., $s_i \in \mathbb{R}^3 \forall i = 1, 2, 3, 4$) from the origin of $\mathcal{F}$ to one of the feature points is assumed to be known. The plane defined by above-the-aisle targets (i.e., the plane defined by the xy-plane of $\mathcal{F}$) and the target feature points is denoted as π. The plane of motion of a WMR is defined by the xy-plane of $\mathcal{I}_{WMR}$, which is coincident with the plane defined by the xy-plane of the greenhouse inertial frame of reference $\mathcal{I}_G$ as depicted in Fig. 2.

Table 1 – List of variables for vision-based WMR state estimation

Motion	Frames	Motion	Frames
R^*, x_f^*	$\mathcal{F}$ to $\mathcal{F}^*$	$R_F(t), x_{fF}(t)$	$\mathcal{F}$ to $\mathcal{I}_F$
R_{RF}^*, x_{fRF}^*	$\mathcal{F}^*$ to $\mathcal{I}_{RF}$	R_{RF}, x_{fRF}	$\mathcal{I}_R$ to $\mathcal{I}_F$
$R_{FRF}(t), x_{fFRF}(t)$	$\mathcal{I}_F$ to $\mathcal{I}_{RF}$	$R_{WMRG}(t), x_{fWMRG}(t)$	$\mathcal{I}_{WMR}$ to $\mathcal{I}_G$
R_c, x_{fc}	$\mathcal{I}_{WMR}$ to $\mathcal{I}_{RF}$	R_G^*, x_{fG}^*	$\mathcal{F}^*$ to $\mathcal{I}_G$
$R_F^*(t), x_{fF}^*(t)$	$\mathcal{F}^*$ to $\mathcal{I}_F$	$R_R^*(t), x_{fR}^*(t)$	$\mathcal{F}^*$ to $\mathcal{I}_R$

The stationary coordinate frame $\mathcal{F}^*$ is attached to the calibrated beginning-of-the-aisle target object, as depicted in Fig. 1, where distance (i.e., $s_i \in \mathbb{R}^3 \forall i = 1, 2, 3, 4$) from the origin of the coordinate frame to one of the feature points is assumed to be known. The four feature points define the plane π^* in Fig. 1. The stationary reference coordinate frames $\mathcal{I}_{RF}$ and $\mathcal{I}_{RR}$ are defined by the forward and reverse looking cameras, respectively, corresponding to the instance when the calibrated target $\mathcal{F}^*$ comes in the field-of-view of forward looking camera (see Fig. 1). The calibrated target $\mathcal{F}^*$ corresponds to a target at the beginning of the aisle while above-the-aisle targets $\mathcal{F}$ are located overhead along the aisle.[2] The position and orientation of the calibrated target $\mathcal{F}^*$ is known with respect to greenhouse inertial frame of reference $\mathcal{I}_G$.

To relate the coordinate systems, let R^*, R_{RF}^*, $R_F^*(t)$, $R_{FRF}(t)$, $R_R^*(t)$, $R_F(t)$, R_{RF}, R_c, R_G^*, $R_{WMRG}(t) \in SO(3)$ denote the rotation from $\mathcal{F}$ to $\mathcal{F}^*$, $\mathcal{F}^*$ to $\mathcal{I}_{RF}$, $\mathcal{F}^*$ to $\mathcal{I}_F$, $\mathcal{I}_F$ to $\mathcal{I}_{RF}$, $\mathcal{F}^*$ to $\mathcal{I}_R$, $\mathcal{F}$ to $\mathcal{I}_F$, $\mathcal{I}_R$ to $\mathcal{I}_F$ (or $\mathcal{I}_{RR}$ to $\mathcal{I}_{RF}$), $\mathcal{I}_{WMR}$ to $\mathcal{I}_{RF}$,$\mathcal{F}^*$ to $\mathcal{I}_G$, and $\mathcal{I}_{WMR}$ to $\mathcal{I}_G$, respectively, $x_f^* \in \mathbb{R}^3$ denotes the translation from $\mathcal{F}$ to $\mathcal{F}^*$ with coordinates expressed in $\mathcal{F}^*$, x_{fRF}^*, $x_{fFRF}(t) \in \mathbb{R}^3$ denotes the respective translation from $\mathcal{F}^*$ to $\mathcal{I}_{RF}$ and $\mathcal{I}_F$ to $\mathcal{I}_{RF}$ with coordinates expressed in $\mathcal{I}_{RF}$, $x_{fF}^*(t)$, $x_{fF}(t)$, $x_{fRF} \in \mathbb{R}^3$ denotes the respective translation from $\mathcal{F}^*$ to $\mathcal{I}_F$, $\mathcal{F}$ to $\mathcal{I}_F$, and $\mathcal{I}_R$ to $\mathcal{I}_F$ (or from $\mathcal{I}_{RR}$ to $\mathcal{I}_{RF}$ expressed in $\mathcal{I}_{RF}$) expressed in $\mathcal{I}_F$, $x_{fR}^*(t) \in \mathbb{R}^3$ denotes the translation from $\mathcal{F}^*$ to $\mathcal{I}_R$ with coordinates expressed in $\mathcal{I}_R$, x_{fG}^*, $x_{fWMRG}(t) \in \mathbb{R}^3$ denotes the respective translation from $\mathcal{F}^*$ to $\mathcal{I}_G$, and $\mathcal{I}_{WMR}$ to $\mathcal{I}_G$ expressed in $\mathcal{I}_G$, and $x_{fc} = [\,x_c \quad y_c \quad z_c\,]^T \in \mathbb{R}^3$ denotes the known constant translation from $\mathcal{I}_{WMR}$ to $\mathcal{I}_{RF}$ expressed in $\mathcal{I}_{RF}$. For clarification, these relationships are represented in a Table 1.

For geometric simplicity in the subsequent analysis, the orientation of calibrated target $\mathcal{F}^*$ is assumed to be the same as orientation of $\mathcal{I}_G$, such that $R_G^* = I^{3\times3}$ and position of $\mathcal{F}^*$ with respect to $\mathcal{I}_G$ given by $x_{fG}^* = [\,x_G^* \quad y_G^* \quad z_G^*\,]^T$ is known. Also, the xy-plane of camera frame $\mathcal{I}_{RF}$ is considered to be parallel to the plane of motion of a WMR. From the geometry between the coordinate frames depicted in Figs. 1 and 2, the following

[1] Image analysis methods can be used to determine planar objects (e.g. through color, texture differences). These traditional computer vision methods can be used to help determine and isolate the four coplanar feature points. If four coplanar target points are not available then the subsequent development can exploit the classic eight-points algorithm (Malis and Chaumette, 2000) with no four of the eight target points being coplanar.

[2] The placement of above-the-aisle targets should be done according to the field-of-view of the monocular camera system, such that at any given instant at least one of the targets is in the field-of-view of the camera system.

relationships can be developed

$$\bar{m}^*_{RFi} = x^*_{fRF} + R^*_{RF}s_i, \qquad \bar{m}^*_{Fi} = x^*_{fF} + R^*_F s_i \tag{1}$$

$$\bar{m}^*_{Ri} = x^*_{fR} + R^*_R s_i, \qquad \bar{m}_{Fi} = x_{fF} + R_F s_i \tag{2}$$

$$\bar{m}^{*'}_{Ri} = x^*_{fR} - x_{fRF} + R^*_R R_{RF} s_i \tag{3}$$

where $\bar{m}^*_{RFi}, \bar{m}^*_{Fi}(t), \bar{m}^*_{Ri}(t) \in \mathbb{R}^3$ denote the Euclidean coordinates of the feature points on the plane π^* expressed in $\mathcal{I}_{RF}$, $\mathcal{I}_F$, and $\mathcal{I}_R$, respectively, as

$$\bar{m}^*_{RFi} \triangleq [\, x^*_{RFi} \quad y^*_{RFi} \quad z^*_{RFi} \,]^T \tag{4}$$

$$\bar{m}^*_{Fi}(t) \triangleq [\, x^*_{Fi}(t) \quad y^*_{Fi}(t) \quad z^*_{Fi}(t) \,]^T \tag{5}$$

$$\bar{m}^*_{Ri}(t) \triangleq [\, x^*_{Ri}(t) \quad y^*_{Ri}(t) \quad z^*_{Ri}(t) \,]^T \tag{6}$$

$\bar{m}_{Fi}(t) \in \mathbb{R}^3$ denotes the time-varying Euclidean coordinates of the feature points on the plane π expressed in $\mathcal{I}_F$ as

$$\bar{m}_{Fi}(t) \triangleq [\, x_{Fi}(t) \quad y_{Fi}(t) \quad z_{Fi}(t) \,]^T \tag{7}$$

$\bar{m}^{*'}_{Ri}(t) \in \mathbb{R}^3$ denotes the time-varying virtual Euclidean coordinates of the feature points on the plane π^* expressed in $\mathcal{I}_F$ as

$$\bar{m}^{*'}_{Ri}(t) \triangleq [\, x^{*'}_{Ri}(t) \quad y^{*'}_{Ri}(t) \quad z^{*'}_{Ri}(t) \,]^T. \tag{8}$$

The Euclidean coordinates $\bar{m}^{*'}_{Ri}(t)$ are referred to as the virtual coordinates since when the WMR translates away from the target $\mathcal{F}^*$ the feature points on the plane π^* cannot be viewed by the forward looking camera $\mathcal{I}_F$ but they are in the field-of-view of reverse looking camera $\mathcal{I}_R$. To facilitate the subsequent development, the normalized Euclidean coordinates of the feature points on the plane π^* can be expressed in terms of $\mathcal{I}_{RF}$, $\mathcal{I}_F$, and $\mathcal{I}_R$ as $m^*_{RFi}, m^*_{Fi}(t)$, and $m^*_{Ri}(t) \in \mathbb{R}^3$, respectively, as follows:

$$m^*_{RFi} \triangleq \frac{\bar{m}^*_{RFi}}{z^*_{RFi}}, \qquad m^*_{Fi}(t) \triangleq \frac{\bar{m}^*_{Fi}(t)}{z^*_{Fi}(t)} \tag{9}$$

$$m^*_{Ri}(t) \triangleq \frac{\bar{m}^*_{Ri}(t)}{z^*_{Ri}(t)}, \qquad m^{*'}_{Ri}(t) \triangleq \frac{\bar{m}^{*'}_{Ri}(t)}{z^{*'}_{Ri}(t)}. \tag{10}$$

Similarly, the normalized Euclidean coordinates of the feature points on the plane π can be expressed in terms of $\mathcal{I}_F$ as follows:

$$m_{Fi} \triangleq \frac{\bar{m}_{Fi}(t)}{z_{Fi}(t)}. \tag{11}$$

Each feature point on the plane π^* will have a projected pixel coordinate expressed in terms of $\mathcal{I}_{RF}$ as

$$p^*_{RFi} \triangleq [\, u^*_{RFi} \quad v^*_{RFi} \quad 1 \,]^T \tag{12}$$

where $p^*_{RFi} \in \mathbb{R}^3$ represents the image-space coordinates of the feature points of the calibrated target $\mathcal{F}^*$, and $u^*_{RFi}, v^*_{RFi} \in \mathbb{R}$. Similarly, the projected pixel coordinate of the Euclidean features on the plane π^* and π can be expressed in terms of $\mathcal{I}_F$ as

$$p^*_{Fi}(t) \triangleq [\, u^*_{Fi}(t) \quad v^*_{Fi}(t) \quad 1 \,]^T, \qquad p_{Fi}(t) \triangleq [\, u_{Fi}(t) \quad v_{Fi}(t) \quad 1 \,]^T \tag{13}$$

where $p^*_{Fi}(t), p_{Fi}(t) \in \mathbb{R}^3$ represents the image-space coordinates of the feature points of the target $\mathcal{F}^*$ and $\mathcal{F}$, respectively, and $u^*_{Fi}(t), v^*_{Fi}(t), u_{Fi}(t), v_{Fi}(t) \in \mathbb{R}$. Also the projected pixel coordinate of the Euclidean features on the plane π^* can be expressed in terms of $\mathcal{I}_R$ as

$$p^*_{Ri}(t) \triangleq [\, u^*_{Ri}(t) \quad v^*_{Ri}(t) \quad 1 \,]^T \tag{14}$$

where $p^*_{Ri}(t) \in \mathbb{R}^3$ represents the image-space coordinates of the feature points of the calibrated target $\mathcal{F}^*$, and $u^*_{Ri}(t), v^*_{Ri}(t) \in \mathbb{R}$. The normalized Euclidean coordinates, $m^*_{RFi}, m^*_{Fi}, m^*_{Ri}$, and m_{Fi}, are related to the corresponding projected pixel coordinates by the pin-hole camera model as

$$p^*_{RFi} = A_F m^*_{RFi}, \qquad p^*_{Fi} = A_F m^*_{Fi} \tag{15}$$

$$p^*_{Ri} = A_R m^*_{Ri}, \qquad p_{Fi} = A_F m_{Fi} \tag{16}$$

where $A_F, A_R \in \mathbb{R}^{3\times3}$ are known, constant, and invertible intrinsic camera calibration matrix corresponding to the forward looking camera and reverse looking camera, respectively.

3. Localization of a WMR

The localization problem is solved considering the four cases corresponding to the possible spatial arrangements of a WMR along the direction of motion in a greenhouse.

3.1. *Case I: Calibrated target $\mathcal{F}^*$ is in the field-of-view of the forward looking camera frame $\mathcal{I}_{RF}$*

This reference location of a WMR corresponds to the instant when the beginning-of-the-aisle calibrated target $\mathcal{F}^*$ comes in the field-of-view of the forward looking on-board camera $\mathcal{I}_{RF}$ (i.e. a snapshot of $\mathcal{F}^*$), the captured target image then is regarded as a reference image. The known distance of the coordinate system $\mathcal{F}^*$ from the xy-plane of $\mathcal{I}_G$ (i.e. the depth of target $\mathcal{F}^*$ from the WMR plane of motion) is given by z^*_G. Also, the distance of $\mathcal{I}_{RF}$ from the WMR plane of motion $\mathcal{I}_{WMR}$ is given by z_c. The unknown depth of the calibrated target frame $\mathcal{F}^*$ from the forward looking camera frame $\mathcal{I}_{RF}$ can be obtained as follows: (see Figs. 1 and 2)

$$z^*_{RFi} = d^*_{RF} = z^*_G - z_c \tag{17}$$

where d^*_{RF} denotes the distance of $\mathcal{F}^*$ from $\mathcal{I}_{RF}$ along the unit normal $n^*_{RF} = [\,0 \quad 0 \quad 1\,]^T$. By using the relationships given in (9), (12), (15), and (17) the Euclidean coordinates $\bar{m}^*_{RFi}$ of the feature points on the plane π^* expressed in $\mathcal{I}_{RF}$ can be determined.

Remark 1. As in Chen et al. (2005), the subsequent development requires that the constant rotation matrix R^*_{RF} be known. The constant rotation matrix R^*_{RF} can be obtained a priori using

various methods (e.g., a second camera, Euclidean measurements) or can be selected as an identity matrix.

Using the first expression (1) and Remark 1, the constant translation x^*_{fRF} between $\mathcal{F}^*$ to $\mathcal{I}_{RF}$ with coordinates expressed in $\mathcal{F}^*$ can be computed. From the coordinate geometry as depicted in Fig. 2, the position and orientation of a WMR coordinate frame $\mathcal{I}_{WMR}$ with respect to the greenhouse inertial frame of reference $\mathcal{I}_G$ can be determined as follows:

$$x_{fWMRG} = x^*_{fG} - x^*_{fRF} - x_{fc} \tag{18}$$

$$R_{WMRG} = R^*_{RF} R_G. \tag{19}$$

3.2. *Case II: Calibrated target $\mathcal{F}^*$ is in the field-of-view of the forward looking camera frame $\mathcal{I}_F$*

This arrangement corresponds to a time-varying trajectory of a WMR when the calibrated target $\mathcal{F}^*$ is in the field-of-view of the forward looking camera frame $\mathcal{I}_F$. The relationship between the Euclidean coordinates $\bar{m}^*_{RFi}$ and $\bar{m}^*_{Fi}(t)$ can be obtained from (1) as follows:

$$\bar{m}^*_{Fi} = x_{fFRF} + R_{FRF}\bar{m}^*_{RFi} \tag{20}$$

where $R_{FRF}(t) \in \mathbb{R}^{3\times3}$ and $x_{fFRF}(t) \in \mathbb{R}^3$, defined in Section 2, are given by

$$R_{FRF} = R^*_F R^{*T}_{RF} \tag{21}$$

$$x_{fFRF} = x^*_{fF} - R_{FRF}x^*_{fRF}. \tag{22}$$

By using the projective relationship (see Figs. 1 and 2)

$$d^*_{RF} = n^{*T}_{RF}\bar{m}^*_{RFi} \tag{23}$$

the relationship in (20) can be expressed as

$$\bar{m}^*_{Fi} = \left(R_{FRF} + \frac{x_{fFRF}}{d^*_{RF}} n^{*T}_{RF}\right)\bar{m}^*_{RFi}. \tag{24}$$

From the expressions given in (9) and (24), the rotation and translation between the coordinate systems $\mathcal{I}_{RF}$ and $\mathcal{I}_F$ can now be related in terms of the normalized Euclidean coordinates as follows:

$$m^*_{Fi} = \underbrace{\frac{z^*_{RFi}}{z^*_{Fi}}}_{\alpha_{FRFi}} \underbrace{(R_{FRF} + x_{hFRF} n^{*T}_{RF})}_{H_{FRF}} m^*_{RFi} \tag{25}$$

In (25), $\alpha_{FRFi}(t) \in \mathbb{R}$ denotes the depth ratio, $H_{FRF}(t) \in \mathbb{R}^{3\times3}$ denotes the Euclidean homography (Faugeras, 2001), and $x_{hFRF}(t) \in \mathbb{R}^3$ denotes the scaled translation vector that is defined as follows:

$$x_{hFRF} = \frac{x_{fFRF}}{d^*_{RF}}. \tag{26}$$

By using (15) and (25), the following relationship can be developed:

$$p^*_{Fi} = \alpha_{FRFi} \underbrace{(A_F H_{FRF} A_F^{-1})}_{G_{FRF}} p^*_{RFi} \tag{27}$$

where $G_{FRF}(t) = [g_{FRFij}(t)] \forall i, j = 1, 2, 3 \in \mathbb{R}^{3\times3}$ denotes the projective homography. Sets of linear equations can be developed from (27) to determine the projective homography up to a scalar multiple. Various techniques can be used (e.g., see Faugeras and Lustman, 2006; Zhang and Hanson, 1995) to decompose the Euclidean homographies, to obtain $\alpha_{FRFi}(t)$, $x_{hFRF}(t)$, $R_{FRF}(t)$. Given that the constant rotation matrix R^*_{RF} is assumed to be known, the expression for $R_{FRF}(t)$ in (21) can be used to determine $R^*_F(t)$. Further $x_{hFRF}(t)$ and the constant translation vector x^*_{fRF}, computed in Section 3.1, can be used to compute the translation $x^*_{fF}(t)$ between $\mathcal{F}^*$ to $\mathcal{I}_F$ expressed in $\mathcal{I}_F$. From the coordinate geometry as depicted in Fig. 2, the position and orientation of a WMR coordinate frame $\mathcal{I}_{WMR}$ with respect to the greenhouse inertial frame of reference $\mathcal{I}_G$ can be determined as follows:

$$x_{fWMRG} = x^*_{fG} - x^*_{fF} - x_{fc} \tag{28}$$

$$R_{WMRG} = R^*_F R^*_G. \tag{29}$$

3.3. *Case III: Calibrated target $\mathcal{F}^*$ is in the field-of-view of the reverse looking camera frame $\mathcal{I}_R$*

This arrangement corresponds to the time-varying trajectory of a WMR such that the calibrated target $\mathcal{F}^*$ is in the field-of-view of the reverse looking camera frame $\mathcal{I}_R$. The relationship between the Euclidean coordinates $\bar{m}^*_{Ri}$ and $\bar{m}^*_{RFi}(t)$ can be obtained from (1) and (2) as follows:

$$\bar{m}^*_{Ri} = x_{fRRF} + R_{RRF}\bar{m}^*_{RFi} \tag{30}$$

where $R_{RRF}(t) \in \mathbb{R}^{3\times3}$ and $x_{fRRF}(t) \in \mathbb{R}^3$, denote the rotation and translation, respectively, between $\mathcal{I}_{RF}$ and $\mathcal{I}_R$ given by

$$R_{RRF} = R^*_R R^{*T}_{RF} \tag{31}$$

$$x_{fRRF} = x^*_{fR} - R_{RRF}x^*_{fRF}. \tag{32}$$

By using the projective relationship stated in (23), the relationship in (30) can be expressed as

$$\bar{m}^*_{Ri} = \left(R_{RRF} + \frac{x_{fRRF}}{d^*_{RF}} n^{*T}_{RF}\right)\bar{m}^*_{RFi}. \tag{33}$$

From the expressions given in (9), (10), and (33), the rotation and translation between the coordinate systems $\mathcal{I}_{RF}$ and $\mathcal{I}_R$ can now be related in terms of the normalized Euclidean coordinates as follows:

$$m^*_{Ri} = \underbrace{\frac{z^*_{RFi}}{z^*_{Ri}}}_{\alpha_{RRFi}} \underbrace{(R_{RRF} + x_{hRRF} n^{*T}_{RF})}_{H_{RRF}} m^*_{RFi}. \tag{34}$$

In (25), $\alpha_{RRFi}(t) \in \mathbb{R}$ denotes the depth ratio, $H_{RRF}(t) \in \mathbb{R}^{3\times3}$ denotes the Euclidean homography, and $x_{hRRF}(t) \in \mathbb{R}^3$ denotes the scaled translation vector that is defined as follows:

$$x_{hRRF} = \frac{x_{fRRF}}{d^*_{RF}}. \tag{35}$$

By using (15), (16), and (34), the following relationship can be developed:

$$p^*_{Ri} = \alpha_{FRFi} \underbrace{(A_R H_{RRF} A_F^{-1})}_{G_{RRF}} p^*_{RFi} \tag{36}$$

where $G_{RRF}(t) = [g_{RRFij}(t)] \forall i, j = 1, 2, 3 \in \mathbb{R}^{3\times3}$ denotes the projective homography. Sets of linear equations can be developed from (36) to determine the projective homography up to a scalar multiple. Various techniques can be used to decompose the Euclidean homographies, to obtain $\alpha_{RRFi}(t)$, $x_{hRRF}(t)$, $R_{RRF}(t)$. Given that the constant rotation matrix R^*_{RF} is assumed to be known, the expression for $R_{RRF}(t)$ in (31) can be used to determine $R^*_R(t)$. Further $x_{hRRF}(t)$ and the constant translation vector x^*_{fRF}, computed in 3.1, can be used to compute the translation $x^*_{fR}(t)$ between $\mathcal{F}^*$ to $\mathcal{I}_R$ expressed in $\mathcal{I}_R$. From the coordinate geometry as depicted in Fig. 2, the position and orientation of a WMR coordinate frame $\mathcal{I}_{WMR}$ with respect to the greenhouse inertial frame of reference $\mathcal{I}_G$ can be determined as follows:

$$x_{fWMRG} = x^*_{fG} - x^*_{fR} - x_{fc} \tag{37}$$

$$R_{WMRG} = R^*_R R^*_G. \tag{38}$$

3.4. *Case IV: Calibrated target $\mathcal{F}^*$ is in the field-of-view of the reverse looking camera frame $\mathcal{I}_R$ and above-the-aisle target $\mathcal{F}$ is in the field-of-view of the forward looking camera frame $\mathcal{I}_F$*

This arrangement represents the pose of a WMR such that the calibrated target $\mathcal{F}^*$ is in the field-of-view of the reverse looking camera frame $\mathcal{I}_R$ and above-the-aisle target $\mathcal{F}$ is in the field-of-view of the forward looking camera frame $\mathcal{I}_F$. The daisy chaining concept (Mehta et al., 2006) is utilized for self-calibration of above-the-aisle targets, in which the position and orientation of above-the-aisle targets (i.e. $\mathcal{F}$) is determined with respect to the greenhouse inertial frame of reference $\mathcal{I}_G$. Using the expressions given in (2) and (3), the relationship between the Euclidean coordinates $\bar{m}^{*'}_{Ri}(t)$ and $\bar{m}^*_{Ri}(t)$ can be stated as follows:

$$\bar{m}^{*'}_{Ri} = R^T_{RF}(\bar{m}^*_{Ri} - x_{fRF}). \tag{39}$$

In (39), the Euclidean coordinates $\bar{m}^*_{Ri}(t)$ can be determined from (24) since the constant Euclidean coordinates $\bar{m}^*_{RFi}$ are found in Section 3.1 and decomposition of homography $H_{RRF}(t)$ yields $R_{RRF}(t)$ and $x_{hRRF}(t)$. Therefore, (39) can be utilized to compute the virtual Euclidean coordinates $\bar{m}^{*'}_{Ri}(t)$ of the feature points on the plane π^* expressed in the camera frame I_F. Also, the expression in (2) yields the following relationship:

$$\bar{m}_{Fi} = x^*_f + R^* \bar{m}^{*'}_{Ri} \tag{40}$$

where $R^*(t)$ and $x^*_f(t)$ denote the time-varying rotation and translation from $\mathcal{F}^*$ to $\mathcal{F}$, as expressed in $\mathcal{F}^*$. Since $\bar{m}^{*'}_{Ri}(t)$ as well as $\bar{m}_{Fi}$ are expressed in I_F, the geometric relationship between the calibrated target $\mathcal{F}^*$ and above-the-aisle target $\mathcal{F}$ can be expressed as follows:

$$\bar{m}_{Fi} = \left(R^* + \frac{x^*_f}{d^*_R} n^{*T}_R \right) \bar{m}^{*'}_{Ri}. \tag{41}$$

From the expression given in (10), the rotation and translation between the coordinate systems $\mathcal{F}^*$ and $\mathcal{F}$ can now be related in terms of the normalized Euclidean coordinates as follows:

$$m_{Fi} = \underbrace{\frac{z^{*'}_{Ri}}{z_{Fi}}}_{\alpha^*_i} \underbrace{(R^* + x^*_h n^{*T}_R)}_{H^*} m^{*'}_{Ri} \tag{42}$$

where $\alpha^*_i(t) \in \mathbb{R}$ denotes the depth ratio, $H^*(t) \in \mathbb{R}^{3\times3}$ denotes the Euclidean homography, and $x^*_h(t) \in \mathbb{R}^3$ denotes the scaled translation vector that is defined as follows:

$$x^*_h = \frac{x^*_f}{d^*_{RF}}. \tag{43}$$

By using (16) and (42), the following relationship can be developed:

$$p_{Fi} = \alpha^*_i \underbrace{(A_F H^* A_F^{-1})}_{G^*} A_F m^{*'}_{Ri} \tag{44}$$

where $G^*(t) = [g^*_{ij}(t)] \forall i, j = 1, 2, 3 \in \mathbb{R}^{3\times3}$ denotes the projective homography. Sets of linear equations can be developed from (44) to determine the projective homography up to a scalar multiple. Various techniques can be used to decompose the Euclidean homographies, to obtain $\alpha^*_i(t)$, $x^*_h(t)$, $R^*(t)$. From the coordinate geometry as depicted in Fig. 2, the position and orientation of above-the-aisle target $\mathcal{F}$ with respect to the greenhouse inertial frame of reference $\mathcal{I}_G$ can be determined as follows:

$$x_{fG} = x^*_{fG} + x^*_f \tag{45}$$

$$R_G = R^* R^*_G. \tag{46}$$

Relationships given in (45) and (46) yield the position and orientation of above-the-aisle target $\mathcal{F}$ with respect to the greenhouse inertial frame $\mathcal{I}_G$. Hence, the above-the-aisle target $\mathcal{F}$ can now be regarded as a calibrated reference target for the localization of a WMR.

4. Experimental results

The experimental results are provided to illustrate the performance of the daisy chaining-based wheeled mobile robot localization scheme. The presented experiment consists of a forward and a reverse looking pin-hole camera mounted on a non-autonomous moving platform looking at the overhanging targets. The hardware for the experimental testbed consists of

the following three main components: (1) forward and reverse looking camera configuration; (2) overhanging targets; and (3) image processing workstation. The cameras used for this configuration are KT&C make (model: KPCS20-CP1) fixed focal length, color CCD cone pinhole cameras. The image output from the cameras is NTSC analog signal which is digitized using universal serial bus (USB) frame grabbers. The overhanging targets are chosen to be planar rectangular patches of size 300 mm × 150 mm and the feature points are considered to be located at the corners of the rectangle, while the targets are placed 411 mm apart from each other. The placement and the size of the target would depend on the selection of a camera. A camera having large field-of-view would require larger targets for better positioning accuracy, but the number of targets required would be less, whereas a camera having larger focal length (i.e., reduced field-of-view) would require smaller targets relatively close to each other while the total number of targets required would depend on the area and the number of aisles of the greenhouse. It has been observed that colored rectangular targets are easy to identify using the traditional image processing algorithms and the required feature points can be selected at the corners of the rectangular target.

The third components is the image processing workstation, which is used for image processing and vision-based state estimation. The image processing workstation operates on a Microsoft Windows XP platform based PC with 3.06 GHz Intel Pentium 4 processor and 768 MB RAM. For the presented experiment, the image processing and state estimation is performed in non-real time using MATLAB.

The intrinsic camera calibration parameters for the forward and reverse looking on-board camera are given as follows: $u_0 = 318$ [pixels] and $v_0 = 247$ [pixels] denote the pixel coordinates of the principal point; $\lambda_1 = 837.98259$ and $\lambda_2 = 771.33238$ denote the product of the focal length and scaling factors, respectively; and $\phi = 0$ [rad] is the skew angle for each camera. The intrinsic camera calibration matrix for the forward and reverse looking camera, denoted as A_f and A_r, respectively, is then given as

$$A_f = A_r = \begin{bmatrix} 837.9826 & 0 & 318 \\ 0 & 771.3324 & 247 \\ 0 & 0 & 1 \end{bmatrix} \tag{47}$$

For simplicity and without loss of generality, the constant known rotation R^*_{RF} between $\mathcal{F}^*$ and $\mathcal{I}_{RF}$ is chosen to be the identity matrix, whereas the constant known rotation R_{RF} and translation x_{fRF} between $\mathcal{I}_F$ and $\mathcal{I}_R$ measured in $\mathcal{I}_F$ are selected as

$$R_{RF} = \begin{bmatrix} 1 & 0 & 0 \\ 0 & 1 & 0 \\ 0 & 0 & 1 \end{bmatrix}, \qquad x_{fRF} = [\,152.4 \quad 0 \quad 0\,]^T. \tag{48}$$

The Euclidean coordinates of the calibrated beginning-of-the-aisle target $\mathcal{F}^*$ with respect to the inertial frame of reference $\mathcal{I}_G$ are measured to be as follows:

$$x^*_{fG} = [\,355 \quad 244 \quad 545\,]^T. \tag{49}$$

4.1. *Case I: Calibrated target $\mathcal{F}^*$ is in the field-of-view of the forward looking camera frame $\mathcal{I}_{RF}$*

The image space coordinates (all image space coordinates are in units of pixels) of the four constant reference target points on the plane π^* as viewed by $\mathcal{I}_{FR}$ are as follows:

$$\begin{aligned} p^*_{RF1} &= [\,425 \quad 289 \quad 1\,]^T \\ p^*_{RF2} &= [\,629 \quad 288 \quad 1\,]^T \\ p^*_{RF3} &= [\,631 \quad 161 \quad 1\,]^T \\ p^*_{RF4} &= [\,415 \quad 152 \quad 1\,]^T. \end{aligned} \tag{50}$$

Utilizing (47), (49), and (50), the Euclidean coordinates of the feature points are given as

$$\begin{aligned} \bar{m}^*_{RF1} &= [\,69.7439 \quad 29.3865 \quad 545\,]^T \\ \bar{m}^*_{RF2} &= [\,202.4197 \quad 28.6800 \quad 545\,]^T \\ \bar{m}^*_{RF3} &= [\,203.7205 \quad -61.0544 \quad 545\,]^T \\ \bar{m}^*_{RF4} &= [\,69.7439 \quad -67.4135 \quad 545\,]^T. \end{aligned} \tag{51}$$

From (1), (18), (19), and (51) the Euclidean position and orientation of a WMR with respect to greenhouse inertial frame of reference $\mathcal{I}_G$ is computed as follows:

$$x_{fWMRG} = [\,215.2561 \quad 262.6135 \quad 0\,]^T \tag{52}$$

$$R_{WMRG} = \begin{bmatrix} 1 & 0 & 0 \\ 0 & 1 & 0 \\ 0 & 0 & 1 \end{bmatrix} \tag{53}$$

The actual measured position and orientation of a WMR with respect to the greenhouse inertial frame of reference is given as below:

$$x_{fWMRG(actual)} = [\,215 \quad 262 \quad 0\,]^T \tag{54}$$

$$R_{fWMRG(actual)} = \begin{bmatrix} 1 & 0 & 0 \\ 0 & 1 & 0 \\ 0 & 0 & 1 \end{bmatrix}. \tag{55}$$

Comparing (52)–(55), it can be identified that the pose of a WMR is identified estimated with significant accuracy. Fig. 3 indicates the actual and the experimentally identified position and orientation of a WMR while the forward looking camera $\mathcal{I}_{RF}$ viewing the calibrated target $\mathcal{F}^*$.

4.2. *Case II: Calibrated target $\mathcal{F}^*$ is in the field-of-view of the forward looking camera frame $\mathcal{I}_F$*

The image space coordinates of the four constant reference target points on the plane π^* as viewed by $\mathcal{I}_F$ for the given instant are measured to be as follows:

$$\begin{aligned} p^*_{F1} &= [\,311 \quad 286 \quad 1\,]^T \\ p^*_{F2} &= [\,533 \quad 287 \quad 1\,]^T \\ p^*_{F3} &= [\,535 \quad 155 \quad 1\,]^T \\ p^*_{F4} &= [\,310 \quad 150 \quad 1\,]^T. \end{aligned} \tag{56}$$

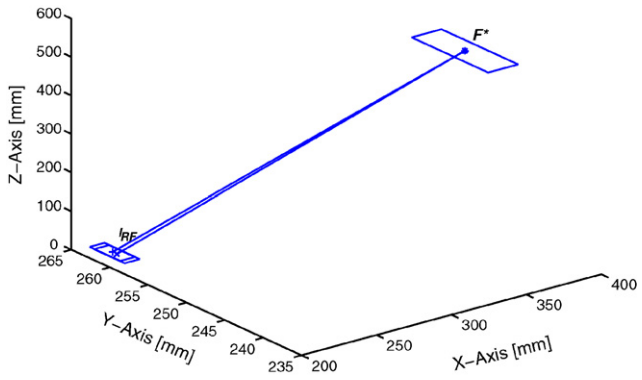

Fig. 3 – Euclidean plot indicating the identified pose of a WMR (denoted by '+'), the actual pose of a WMR $\mathcal{I}_{RF}$ (denoted by 'x') while viewing the target $\mathcal{F}^*$ (denoted by '*') by the forward looking camera.

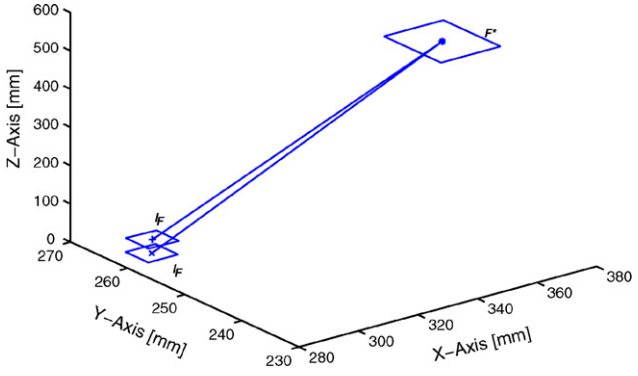

Fig. 4 – Euclidean plot indicating the identified pose of a WMR (denoted by '+'), the actual pose of a WMR $\mathcal{I}_F$ (denoted by 'x') while viewing the target $\mathcal{F}^*$ (denoted by '*') by the forward looking camera.

Substituting (50) and (56), the decomposition of homography given in (25) yields the rotation $R_{FRF}(t)$, translation $x_{fFRF}(t)$, unit normal to the plane π^*, and depth ratio $\alpha_{FRFi}(t)$ as follows:

$$\begin{aligned} R_{FRF} &= \begin{bmatrix} 0.997305 & 0.017191 & -0.021936 \\ -0.016461 & 0.999602 & -0.021936 \\ -0.017390 & 0.021835 & 0.997198 \end{bmatrix} \\ x_{fFRF} &= [-91 \quad 12 \quad 0]^T \\ \alpha_{FRF1} &= 1.000564, \quad \alpha_{FRF2} = 1.040473 \\ \alpha_{FRF3} &= 1.064294, \quad \alpha_{FRF4} = 1.024555 \\ n^*_{RF} &= [0.00015591 \quad 0.00039507 \quad 1]. \end{aligned} \tag{57}$$

Utilizing (2), (30), (21), (22), (51), and (57), the Euclidean pose of a WMR is computed as follows:

$$x_{fWMRG} = [297.6723 \quad 264.8610 \quad 4.3637]^T \tag{58}$$

$$R_{WMRG} = \begin{bmatrix} 0.9973 & 0.0172 & 0.0170 \\ -0.0165 & 0.9996 & -0.0219 \\ -0.0174 & 0.0218 & 0.9972 \end{bmatrix}. \tag{59}$$

The actual measured position and orientation of a WMR with respect to the greenhouse inertial frame of reference is as follows:

$$x_{fWMRG(actual)} = [292 \quad 262 \quad 0]^T \tag{60}$$

$$R_{WMRG(actual)} = \begin{bmatrix} 1 & 0 & 0 \\ 0 & 1 & 0 \\ 0 & 0 & 1 \end{bmatrix}. \tag{61}$$

From (58)–(61), it can be seen that the pose of a WMR has been successfully identified. Fig. 4 indicates the actual and the experimentally identified position and orientation of a WMR while the forward looking camera $\mathcal{I}_F$ viewing the calibrated target $\mathcal{F}^*$.

4.3. *Case III: Calibrated target $\mathcal{F}^*$ is in the field-of-view of the reverse looking camera frame $\mathcal{I}_R$*

The image space coordinates of the four constant reference target points on the plane π^* as viewed by $\mathcal{I}_R$ for the given instant are measured to be as follows:

$$\begin{aligned} p^*_{R1} &= [14 \quad 304 \quad 1]^T \\ p^*_{R2} &= [219 \quad 306 \quad 1]^T \\ p^*_{R3} &= [217 \quad 171 \quad 1]^T \\ p^*_{R4} &= [11 \quad 177 \quad 1]^T. \end{aligned} \tag{62}$$

Using (50) and (62), the decomposition of homography given in (34) yields the rotation $R_{RRF}(t)$, translation $x_{fRRF}(t)$, unit normal to the plane π^*, and depth ratio $\alpha_{RRFi}(t)$ as follows:

$$\begin{aligned} R_{RRF} &= \begin{bmatrix} 0.998597 & 0.094310 & 0.077288 \\ -0.094355 & 0.995497 & -0.018622 \\ -0.078687 & 0.011477 & 1.002996 \end{bmatrix} \\ x_{fRRF} &= [-305.8 \quad 12 \quad 0]^T \\ \alpha_{FRF1} &= 1.000564, \quad \alpha_{FRF2} = 1.040473 \\ \alpha_{FRF3} &= 1.064294, \quad \alpha_{FRF4} = 1.024555 \\ n^*_{RF} &= [8.7518 \times 10^{-6} \quad 0.00043127 \quad 1]. \end{aligned} \tag{63}$$

Utilizing (1), (20), (31), (32), (51), and (63), the Euclidean pose of a WMR can be identified as follows:

$$x_{fWMRG} = [480.8930 \quad 273.8639 \quad 9.5768]^T \tag{64}$$

$$R_{FRF} = \begin{bmatrix} 0.9986 & 0.0943 & 0.0773 \\ -0.0944 & 0.9955 & -0.0186 \\ -0.0787 & 0.0115 & 1.0030 \end{bmatrix}. \tag{65}$$

The actual measured position and orientation of a WMR with respect to the greenhouse inertial frame of reference is as follows:

$$x_{fWMRG(actual)} = [493 \quad 262 \quad 0]^T \tag{66}$$

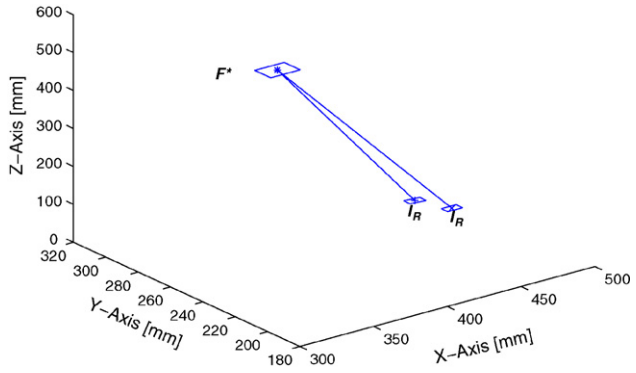

Fig. 5 – Euclidean plot indicating the identified pose of a WMR $\mathcal{I}_R$ (denoted by '+'), the actual pose of a WMR $\mathcal{I}_R$ (denoted by 'x') while viewing the target $\mathcal{F}^*$ (denoted by '*') by the reverse looking camera.

$$R_{WMRG(actual)} = \begin{bmatrix} 1 & 0 & 0 \\ 0 & 1 & 0 \\ 0 & 0 & 1 \end{bmatrix}. \tag{67}$$

Comparing (64)–(67), it can be seen that the pose of a WMR has been identified with sufficient accuracy. Fig. 5 indicates the actual and the experimentally identified position and orientation of a WMR while the reverse looking camera $\mathcal{I}_R$ viewing the calibrated target $\mathcal{F}^*$.

4.4. *Case IV: Calibrated target $\mathcal{F}^*$ is in the field-of-view of the reverse looking camera frame $\mathcal{I}_R$ and above-the-aisle target $\mathcal{F}$ is in the field-of-view of the forward looking camera frame $\mathcal{I}_F$*

The image space coordinates of the four constant reference target points on the planes π^* and π as viewed by $\mathcal{I}_R$ and $\mathcal{I}_F$, respectively, for the given instant are measured to be as follows:

$$\begin{aligned} p^*_{R1} &= [14 \quad 304 \quad 1]^T \\ p^*_{R2} &= [219 \quad 306 \quad 1]^T \\ p^*_{R3} &= [217 \quad 171 \quad 1]^T \\ p^*_{R4} &= [11 \quad 177 \quad 1]^T. \end{aligned} \tag{68}$$

$$\begin{aligned} p_{F1} &= [397 \quad 306 \quad 1]^T \\ p_{F2} &= [608 \quad 306 \quad 1]^T \\ p_{F3} &= [612 \quad 179 \quad 1]^T \\ p_{F4} &= [400 \quad 172 \quad 1]^T. \end{aligned} \tag{69}$$

Using (39) the virtual pixel coordinates of the target points on the plane π^* are obtained for the forward looking on-board camera as follows:

$$\begin{aligned} p^{*'}_{R1} &= [-214.0880 \quad 282.3448 \quad 1]^T \\ p^{*'}_{R2} &= [-15.5866 \quad 263.8270 \quad 1]^T \\ p^{*'}_{R3} &= [-27.5935 \quad 133.6519 \quad 1]^T \\ p^{*'}_{R4} &= [-229.3023 \quad 144.8639 \quad 1]^T. \end{aligned} \tag{70}$$

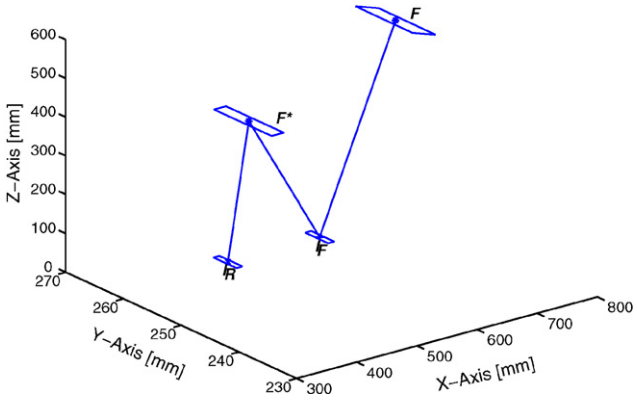

Fig. 6 – Euclidean plot indicating the identified position and orientation of above-the-aisle target $\mathcal{F}$ (denoted by '*'), while the forward looking camera $\mathcal{I}_F$ (denoted by '+') viewing the target $\mathcal{F}$ and the reverse looking camera $\mathcal{I}_R$ viewing the calibrated target $\mathcal{F}_*$ (denoted by 'x').

Using (69) and (70), the decomposition of homography given in (42) yields the rotation R^*, translation x^*_h, and depth ratio α^*_i as follows:

$$\begin{aligned} R^* &= \begin{bmatrix} 1.0683 & -0.0816 & -0.0249 \\ 0.0885 & 0.9967 & 0.0026 \\ 0.0246 & -0.0063 & 1.0720 \end{bmatrix} \\ x^*_f &= [393.6373 \quad 15.6168 \quad -13.0245]^T \\ \alpha_1 &= 0.969647, \quad \alpha_2 = 0.971852 \\ \alpha_3 &= 0.965629, \quad \alpha_4 = 0.963069. \end{aligned} \tag{71}$$

Utilizing (45), (46), and (71), the Euclidean position and orientation of above-the-aisle target $\mathcal{F}$ with respect to the greenhouse inertial frame of reference is computed as follows:

$$x_{fG} = [748.6373 \quad 259.6168 \quad 531.9755]^T \tag{72}$$

$$R_G = \begin{bmatrix} 1.0683 & -0.0816 & -0.0249 \\ 0.0885 & 0.9967 & 0.0026 \\ 0.0246 & -0.0063 & 1.0720 \end{bmatrix} \tag{73}$$

The actual measured position and orientation of the target $\mathcal{F}$ with respect to the greenhouse inertial frame of reference is as follows:

$$x_{fG(actual)} = [766 \quad 244 \quad 549]^T \tag{74}$$

$$R_{G(actual)} = \begin{bmatrix} 1 & 0 & 0 \\ 0 & 1 & 0 \\ 0 & 0 & 1 \end{bmatrix}. \tag{75}$$

Comparing (72)–(75), it can be seen that the position and orientation of the target $\mathcal{F}$ has been successfully identified. Fig. 6 indicates the experimentally identified position and orientation of above-the-aisle target $\mathcal{F}$ while the forward looking camera $\mathcal{I}_F$ viewing the target $\mathcal{F}$ and reverse looking camera $\mathcal{I}_R$ viewing the calibrated target $\mathcal{F}^*$.

Thus, it can be seen that using equations (18), (19), (28), (29), (37), and (38) the states of the WMR can be estimated and

hence the position and orientation of the WMR can be identified. Also, the position and orientation of above-the-aisle target $\mathcal{F}$ can be identified using (45) and (46) and hence the target $\mathcal{F}$ can be considered as a calibrated target for further state estimation of a WMR. However, any errors in the measurement of the pose of beginning-of-the-aisle reference target and onboard camera location with respect to a WMR reference frame would result in a WMR localization error. Moreover, errors involved in the camera calibration parameters and pixel resolution can lead to the WMR state estimation errors. Typically, these errors can be minimized by accurate positioning of the beginning-of-the-aisle reference target, extensive evaluation of the intrinsic and extrinsic camera calibration parameters, sub-pixel image processing, and using high resolution image sensors

5. Conclusion

In this paper, the position and orientation of a WMR is identified with respect the greenhouse inertial frame of reference using a vision-based state estimation strategy. To achieve the result, multiple views of a reference objects were used to develop Euclidean homographies. By decomposing the Euclidean homographies into separate translation and rotation components, reconstructed Euclidean information was obtained for calibration of unknown targets for localization of a WMR. The impact of this paper is a new framework to identify the pose of a moving WMR through images acquired by a moving camera, which would be beneficial for spatial selection and autonomous operations in a greenhouse. Experimental results verify the daisy chaining-based approach for localization scheme presented in this paper.

REFERENCES

Acaccia, G.M., Michelini, R.C., Molfino, R.M., Razzoli, R.P., 2003. Mobile robots in greenhouse cultivation: inspection and treatment of plants. In: Proceedings of ASER 1st International Workshop on Advances in Service Robotics, Italy.

Aono, T., Fujii, K., 1988. Position of vehicle on undulating ground using GPS and dead reckoning. In: Proceedings of IEEE International Conference on Robotics and Automation, pp. 3443–3448.

Ashokaraj, I., Tsourdos, A., Silson, P., White, B., Economou, J., 2004. Feature based robot navigation: using fuzzy logic and interval analysis. In: Proceedings of IEEE International Conference on Fuzzy Systems, vol. 3, pp. 1461–1466.

Badgery-Parker, J., 1999. Agnote DPI/249. Edition 1, pp. 1–2.

Chen, J., Dawson, D.M., Dixon, W.E., Behal, A., 2005. Adaptive homography-based visual servo tracking for fixed and camera-in-hand configurations. IEEE Trans. Control Syst. Technol. 13 (5), 814–825.

Dario, P., Sandini, G., Allotta, B., Bucci, A., Buemi, F., Massa, M., Ferrari, F., Magrassi, M., Bosio, L., Valleggi, R., Gallo, E., Bologna, A., Cantatore, F., Torrielli, G., Mannucci, A., 1994. The Agribot Project for greenhouse automation. In: Proceedings of International Symposium on New Cultivation Systems in Greenhouse, vol. 361, Italy, pp. 85–92.

Faugeras, O., 2001. Three-Dimensional Computer Vision. The MIT Press, Cambridge, MA.

Faugeras, O., Lustman, F., 2006. Motion and structure from motion in a piecewise planar environment. Int. J. Comput. Vision 37 (1), 79–97.

Guo, X., Qu, Z., Xi, B., 2006. Research on location method for mobile robots formation based on global-camera. In: Proceedings of International Symposium on Systems and Control in Aerospace and Astronautics, pp. 347–349.

Hada, Y., Takase, K., 2001. Multiple mobile robot navigation using the indoor global positioning system (iGPS). In: Proceedings of International Conference on Intelligent Robots and Systems, vol. 2, pp. 1005–1010.

ldzikowski, M., Nowakowski, J., Podsedkowski, L., Visvary, I., 1999. On-line navigation of mobile robots using laser scanner. In: Proceedings of International Workshop on Robot Motion and Control, pp. 241–245.

Idzikowski, M., Podsedkowski, L., 2005. Simulation and experimental results of a new method of mobile robot localization. In: Proceedings of 5th International Workshop on Robot Motion and Control, pp. 175–179.

Kleeman, L., Kuc, R., 1995. Mobile robot sonar for target localization and classification. Int. J. Robot. Res. 14 (4), 295–318.

Malis, E., Chaumette, F., 2000. 2 1/2 D visual servoing with respect to unknown objects through a new estimation scheme of camera displacement. Int. J. Comput. Vision 37 (1), 79–97.

Mehta, S.S., Dixon, W.E., MacArthur, D., Crane, C.D., 2006. Visual servo control of an unmanned ground vehicle via a moving airborne monocular camera. In: Proceedings of IEEE American Control Conference, Minnesota, pp. 5276–5281.

Ohno, K., Tadokoro, S., 2005. Dense 3D map building based on LRF data and color image fusion. In: Proceedings of IEEE Conference on Intelligent Robotics and Systems, pp. 2792–2797.

Sammons, P.J., Furukawa, T., Bulgin, A., 2005. Autonomous pesticide spraying robot for use in a greenhouse. In: Proceedings of the Australasian Conference on Robotics & Automation, Australia.

Skrzypczyfnski, P., Drapikowski, P., 1999. Environment modelling in a multi-agent mobile system. In: Proceedings of 3rd European Workshop on Advanced Mobile Robots, pp. 41–48.

Tsai, C., 1998. A localization system of B mobile robot by fusing dead reckoning and ultrasonic measurements. IEEE Trans. Instrum. Meas. 47 (5), 1399–1404.

Van Henten, E.J., Van Tuijl, B.A.J., Hoogakker, G.J., Van Der Weerd, M.J., Hemming, J., Kornet, J.G., Bontsema, J., 2004. An autonomous robot for de-leafing cucumber plants grown in a high-wire cultivation system. In: Proceedings of ISHS International Conference on Sustainable Greenhouse Systems, vol. 691, Belgium, pp. 877–884.

Yamaucbi, B., 1996. Mobile robots localization in dynamic environments using dead reckoning and evidence grids. In: Proceedings of IEEE International Conference on Robotics and Automation, pp. 1401–1406.

Zhang, Z., Hanson, A.R., 1995. Scaled Euclidean 3D reconstruction based on externally uncalibrated cameras. In: IEEE Symposium on Computer Vision, pp. 37–42.

Zhang, L., Ghosh, B.K., 2000. Line segment based map building and localization using 2D laser rangefinder. In: Proceedings of IEEE International Conference on Robotics and Automation, vol. 3, pp. 2538–2543.